Emergent superconductivity from suppression of charge order in pressurized Re_3Ge_7

Yang Zhang,[1,*] Xiupeng Sun,[2,3,*] Chunhui Ye,[1] Hongze Zhao,[1] Rucheng Dai,[4] Zhongping Wang,[5] Junfeng He,[2,3,†] and Zengming Zhang[1,3,5,‡]

[1]*Deep Space Exploration Laboratory/Department of Physics, School of Physical Sciences, University of Science and Technology of China, Hefei 230026, China*

[2]*Department of Physics, University of Science and Technology of China, Hefei, Anhui 230026, China*

[3]*CAS Key Laboratory of Strongly-coupled Quantum Matter Physics, University of Science and Technology of China, Hefei, Anhui 230026, China*

[4]*Deep Space Exploration Laboratory/The Centre for Physical Experiments, University of Science and Technology of China, Hefei, Anhui 230026, China*

[5]*The Centre for Physical Experiments, University of Science and Technology of China, Hefei, Anhui 230026, China*

(Received 10 May 2023; accepted 16 November 2023; published 6 December 2023)

The emergence of superconductivity is often accompanied by competing charge/magnetic orders, such as charge/spin density waves and antiferromagnetism in correlated systems. The superconducting temperature T_C can often be significantly enhanced once the competing order is suppressed via external stimuli. Recently, Re_3Ge_7 has attracted considerable attention due to its temperature-induced metal-insulator-like transition, which is inexplicably related to superconductivity. In this study, we have discovered that Re_3Ge_7 single crystals exhibit pressure-induced superconductivity due to the suppression of charge order. Re_3Ge_7 displays an insulatorlike upturn of electronic resistivity bellow 60 K at ambient pressure without triggering a structure transition. The dominant carrier changes from electrons to holes at low temperatures. The temperature-dependent angle-resolved photoemission spectroscopy investigations indicated that the band structure of Re_3Ge_7 does not appear to alter significantly between 70 K and 7 K. After ruling out some possible competing orders based on experimental evidence, we suggest that the insulatorlike state could be the unconventional charge ordering's plausible ground state. Our findings indicate that the emergence of superconductivity can be achieved at a relatively low pressure of 0.2 GPa by restraining the charge order. With increasing pressure, T_C is slightly enhanced, reaching a maximum value of 5.3 K at 24.1 GPa, while the charge order is rapidly inhibited until it becomes imperceptible. The superconductivity shows an unusual platform-shaped phase diagram, suggesting the possibility of unconventional electronic contributions. The current research poses important questions concerning the Re_3Ge_7 unconventional charge order and how it competes with the appearance of superconductivity.

DOI: 10.1103/PhysRevB.108.224504

I. INTRODUCTION

One of the most critical challenges in condensed matter physics is the competition between various ground orders in a many-body electron system. For example, it has been discovered through research on representative unconventional superconductors such as cuprates, iron-pnictides, and heavy-fermion superconductors that superconducting states and other electronic-driven states are always in a complicated competition and have the potential to combine to create new superconductivity [1–8]. Exploring the complicated interplay between superconductivity and opposing orders has become a major focus on the superconductivity physics frontiers [9–13]. Efficient strategies for manipulating the competing charge/magnetic orders and seeking for the superconductivity ground state within materials include physical/chemical pressure and carrier doping [6,12,14–17]. In contrast to the internal compression caused by chemical doping, applying external pressure is a clean procedure without introducing chemical disorder [18–22]. Interestingly, the competition between electronic-driven state and superconductivity occurs regularly under pressure in some cuprates [16], iron-based superconductors [23], and other materials [8,24,25]. Recent advances in kagome CsV_3Sb_5 have unveiled a possible stripelike charge density wave (CDW) order arising between 0.58 GPa and 2.0 GPa, which leads to the unusual two-dome-like superconducting behavior under pressure [22]. Additionally, a new nickelate superconductor with T_C close to 80 K has been discovered recently via application of pressure [8].

Re_3Ge_7 single crystals are hard to synthesize, since the eutectic temperature region of Re-Ge system is quite narrow [26–29]. It has an orthorhombic structure with space group *Cmcm* [26]. The magnetization characterization reveals a weak diamagnetic ground state. More intriguingly, a sharp increase in electrical resistivity below 60 K reveals a metal-insulator-like transition. The discovery of a kink in magnetic

*Y. Zhang and X. Sun contributed equally to this work.
†Corresponding author: jfhe@ustc.edu.cn
‡Corresponding author: zzm@ustc.edu.cn

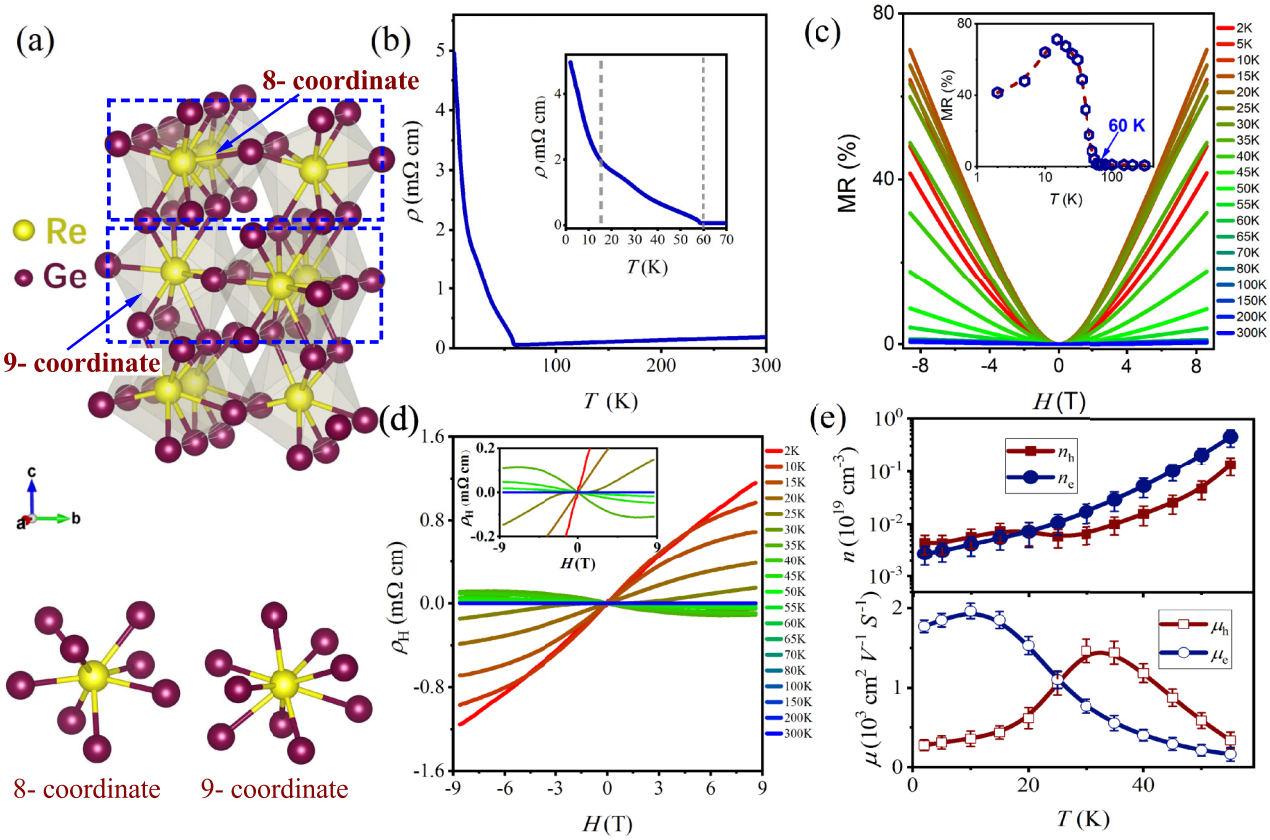

FIG. 1. Crystal structure and transport properties of Re_3Ge_7 at ambient pressure. (a) Schematic diagram of the crystal structure of Re_3Ge_7. The bottom half describes the eight- and nine-geometries bonding between Re atoms and Ge atoms. (b) Resistivity as a function of temperature at ambient pressure. The illustration highlights the low-temperature section, showing insulatorlike behavior below 60 K. (c) MR as a function of external magnetic field at various temperatures from 2–300 K. The inset shows the MR *vs* temperature at 9 T, revealing a steep ascent below 60 K with a summit around 15 K. (d) The Hall resistivity ρ_H as a function of magnetic field at various temperatures. The inset shows the details of Hall resistivity at typical temperatures. (e) Extracted carrier concentration n and mobility μ as a function of temperature.

susceptibility and a λ-like anomaly in specific heat at the critical temperature confirms the presence of a phase transition [27]. The temperature-dependent powder x-ray diffraction investigation shows a sudden change in unit cell parameters without symmetry variation near the transition temperature, demonstrating the transition's second-order nature. The electronic structure calculations suggest a gap opening around the Fermi level right above the narrow pocket of strong $5d$-$4p$ hybridized states, which might be responsible for the insulatorlike state [29]. Moreover, substitution of Ga for Ge leads to a suppression of the insulatorlike ground state and emergence of superconductivity. The superconducting temperature T_C shows a typical domelike doping dependence with a maximum value of 3.37 K for $Re_3Ge_{7-x}Ga_x$ with $x = 0.25$ [28]. Furthermore, Re_3Ge_7 is also proposed to be a topological high-symmetry point semimetal [30]. These unusual properties have led to greater curiosity about the nature of its insulatorlike state and its connection to the superconducting order.

In this paper, we perform angle-resolved photoemission spectroscopy (ARPES) and high-pressure transport studies on high-quality Re_3Ge_7 single crystals. The absence of evident band gap after the metal-insulator-like transition in ARPES experiment distinguishes it from the typical band-gapped insulating state, thus a possible unconventional charge-driven state is discussed. Furthermore, high-pressure electrical resistivity experiments show the emergence of superconductivity via the suppression of such charge order at extremely low pressure. Our work sheds light on the ground nature of the localized charge ordering in Re_3Ge_7 and its competitive relationship with emergent superconductivity.

II. RESULTS AND DISCUSSION

Structure, ambient pressure transport, and ARPES characterization. Single-crystal x-ray diffraction (SC-XRD) measurements of the as-prepared Re_3Ge_7 is carried out and analyzed to obtain the precise crystal structure. The crystal parameters from SC-XRD refinement are displayed in Table S1 of the Supplemental Material [31]. The lattice parameters of the orthorhombic structure are $a = 3.2280(3)$ Å, $b = 9.0454(8)$ Å, and $c = 21.9438(19)$ Å, which show good agreement with previous reports [26,27]. Figure 1(a) shows a schematic diagram of the crystal structure for Re_3Ge_7. Orthorhombic Re_3Ge_7 is rather unique, with no isostructural analogs. There are two inequivalent Re sites and four inequivalent Ge sites. The two inequivalent Re atoms are bonded in eight- and nine-coordinate geometries to Ge atoms, as shown

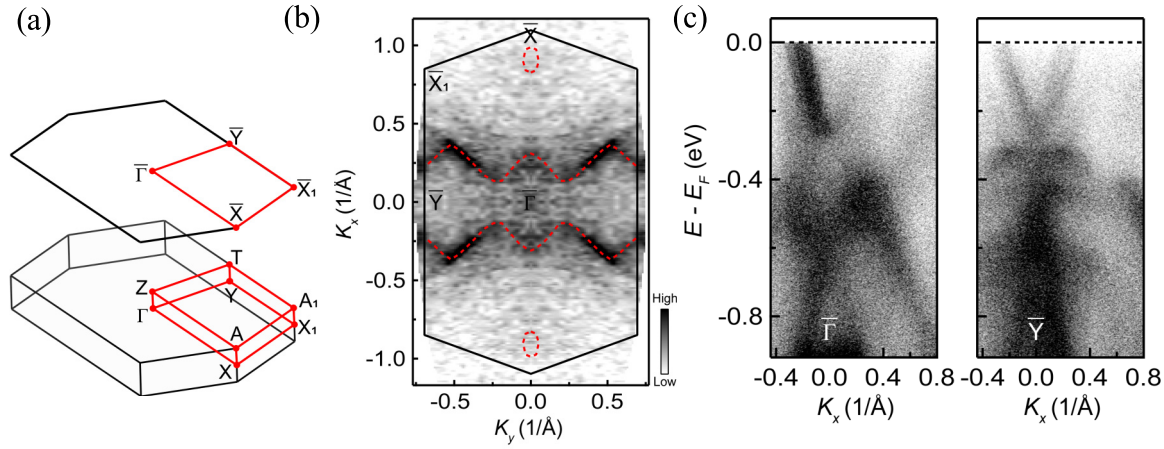

FIG. 2. ARPES results of Re_3Ge_7. (a) The three-dimensional (3D) Brillouin zone of primitive cell and the projected in-plane Brillouin zone with high-symmetry points indicated. (b) Fermi surface of Re_3Ge_7 measured by ARPES with 21.2 eV photons at 7 K. The dashed lines are guides to the eye. (c) Band structures along $\bar{X}$-$\bar{\Gamma}$-$\bar{X}$ (left) and $\bar{X}_1$-$\bar{Y}$-$\bar{X}_1$ (right) directions measured by ARPES at 7 K.

in the bottom half of Fig. 1(a). The corrugated nets formed by the Ge atoms are located right between the Re-based trigonal prisms' layers.

The electrical resistivity, $\rho(T)$, of the Re_3Ge_7 single crystal is shown against temperature from 1.8–300 K at ambient pressure in Fig. 1(b). The $\rho(T)$ initially decreases monotonously with cooling before abruptly increasing at 60 K, exhibiting a similar metal-insulator-like transition with prior results [27–29]. It is also important to note that with further cooling, $\rho(T)$ undergoes a steeper rise at around 15 K, as illustrated in the inset of Fig. 1(b). Fig. 1(c) depicts the magnetoresistivity [(MR), $[\rho(H) - \rho(0)]/\rho(0)$] at various temperatures, revealing a nonsaturated trend up to 9 T at low temperatures. The MR curves in the high-field region exhibit a nearly linear field dependence. The inset of Fig. 1(c) shows MR as a temperature function at a 9 T field. The MR is, as can be shown, extremely small in the metallic state above 60 K. However, below 60 K, MR increases dramatically, reaching a maximum value of approximately 71% at 15 K, where $\rho(T)$ commences its second rapid ascent. Moreover, the Hall resistivity ρ_H exhibits apparent bending around 60 K as shown in Fig. 1(d), suggesting multiband behavior. According to the classic two-carriers transport model, the field-dependent ρ and ρ_H can be expressed as follows:

$$\rho(B) = \frac{1}{e}\left[\frac{n_e\mu_e + n_h\mu_h + (n_e\mu_h + n_h\mu_e)\mu_e\mu_h B^2}{(n_e\mu_e + n_h\mu_h)^2 + (n_h - n_e)^2\mu_e^2\mu_h^2 B^2}\right] \quad (1)$$

$$\rho_H(B) = \frac{B}{e}\left[\frac{n_h\mu_h^2 - n_e\mu_e^2 + (n_h - n_e)\mu_e^2\mu_h^2 B^2}{(n_e\mu_e + n_h\mu_h)^2 + (n_h - n_e)^2\mu_e^2\mu_h^2 B^2}\right] \quad (2)$$

where (n_e, μ_e) and (n_h, μ_h) are the carrier concentrations and mobilities for electron and hole, respectively. The extracted n_e, n_h μ_e, and μ_h as a function of temperature are shown in Fig. 1(e). The carrier concentrations n_h and n_e intersect in the vicinity near 20 K, indicating a change in carrier type from electron to hole. This critical temperature is consistent with the temperature at which MR reaches its maximum value at 9 T, and the Hall coefficient reverses sign. The carrier mobilities μ_h and μ_e exhibit no distinction in the order of magnitude below 60 K. Similar phenomena have been reported in $ZrTe_5$, where the Hall coefficient undergoes sign reversal and exhibits multiband characteristics due to temperature-induced Lifshitz phase transition [32,33]. We noticed that similar field-induced MR maximum and linear MR dependency have also been identified in CDW $LaSb_2$ and half-Heusler compound RPtBi (R = Dy, Gd, and Nd), whose intrinsic origins are attributed to possible field-induced density wave transition and temperature-driven band crossing [34–38]. All anomalies in the transport behaviors of Re_3Ge_7 consistently point to an unusually ordered state at low temperatures.

The ARPES experiments were carried out to investigate the electronic band structure of Re_3Ge_7. Figure 2(a) describes the 3D Brillouin zone and the projected in-plane Brillouin zone of Re_3Ge_7, with crucial high-symmetry points. Figure 2(b) depicts the Fermi surface measured by ARPES using 21.2 eV photons at 7 K. Figure 2(c) shows the measured band structures along the $\bar{X}$-$\bar{\Gamma}$-$\bar{X}$ and $\bar{X}_1$-$\bar{Y}$-$\bar{X}_1$ directions at 7 K, in accordance with the theoretical calculated electronic band structure [29]. The band structures along these two directions at 40 K and 70 K are provided in Figs. S1 and S2 of the Supplemental Material [31]. In addition, the band structure and Fermi surface show no topological change with decreasing temperature in the measurement. Consequently, there is no evidence of a gap opening in Re_3Ge_7 at low temperature, indicating that the ground state of Re_3Ge_7 should not be considered as a simple band-gapped insulating phase. Previous low-temperature structural studies have revealed abrupt changes in lattice parameters without the emergence of a phase transition [29], which is consistent with our low-temperature XRD results as shown in Fig. S3 [31]. Furthermore, the weak diamagnetism negates the possibility of long-range spin order formation [27]. Therefore, the anomaly observed below 60 K will likely stem from an unconventional state of charge order, which may also interact with topological order. [30,39,40].

Pressure-induced superconductivity. Figures 3(a) and 3(b) depict the evolution of electrical resistivity ρ for Re_3Ge_7 with the application of pressure in two runs, focusing on low-pressure and high-pressure ranges, respectively. Surprisingly, after applying only 0.2 GPa of pressure, an obvious drop

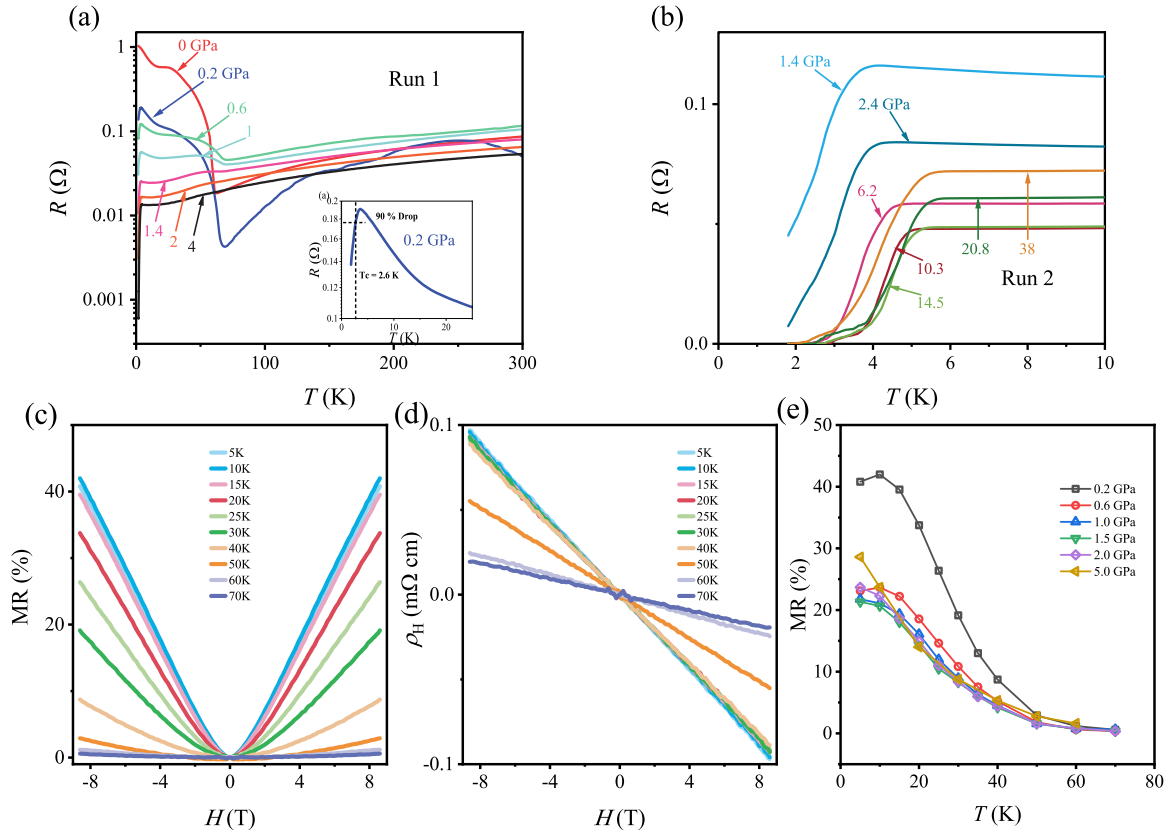

FIG. 3. Transport properties of Re_3Ge_7 at high pressure. (a) ρ-T curves with pressure ranging from 0–4 GPa in run 1. The illustration enlarges the first sign of superconductivity at 0.2 GPa. It should be noted that, due to low pressure and poor contact between electrodes and samples in local areas, the resistivity at 0.2 GPa fluctuates significantly with temperature. (b) ρ-T curves with pressure ranging from 1.4–38 GPa at low-temperature region in run 2. (c) MR from 5–70 K at 0.2 GPa. The critical temperature of MR maximum is suppressed to around 10 K. (d) Hall resistivity ρ_H from 5–70 K at 0.2 GPa, showing vanishing of bending and sign reversal. These phenomena clearly demonstrate that the charge-ordered ground state has been inhibited. (e) MR as a function of temperature at various pressures. With rising pressure, the MR maximum collapses and shifts to lower temperature, clearly stating a dampening influence of the charge order.

in resistivity appears above the cryostat's lowest temperature of 1.8 K, demonstrating pressure-induced superconductivity. In addition, superconducting transition temperature T_C, defined as 90% drop of the normal-state resistivity [18,19,41], is determined to be 2.6 K, as illustrated in the inset of Fig. 3(a). Generally, the normal state of superconductor is metal, the resistivity decreases with the temperature. In the current case, it is insulatorlike state below 60K, which shows a unique superconductivity in an insulatinglike state. With further increasing pressure, the substantial up warp at low temperature in ρ-T curve progressively lessens, indicating that the material's insulatorlike behavior is significantly suppressed, which restrains charge order. This suppression is further supported by the receding present temperature of charge-order-related MR maximum and Hall anomalies with pressure. Figures 3(c) and 3(d) show the MR and Hall results at 0.2 GPa from 5–70 K. With a loading of only 0.2 GPa, the temperature of the MR maximum at 9 T has fallen to around 10 K. Additionally, the Hall resistivity loses its bending and sign reversion characteristics at ambient pressure, the signal is reduced to an ordinary Hall signal and the Hall coefficient remains negative, indicating that the carrier type becomes electron. As shown in Fig. 3(e), as pressure rises from 0.2 GPa, the MR maximum continuously diminishes and disappears near 5 GPa. Around this critical pressure, the charge-ordered insulatorlike behavior in the ρ-T curve becomes practically indistinguishable, and the sample exhibits a metallic scenario above the superconducting state. Meanwhile, T_C rises marginally with increasing pressure, peaking at 5.3 K at 24.1 GPa. The superconductivity survived to the experimentally reached maximum pressure of 38 GPa, with no appreciable drop in T_C. Re_3Ge_7 distinguishes itself from other pressure-induced dome-type superconductivity by maintaining a virtually consistent T_C across such a broad range. The zero resistivity is achieved for pressures higher than 6.2 GPa. Ultimately, during decompression process, T_C shares the similar trends with compression, suggesting the reversibility of the pressure tuning the superconducting order in Re_3Ge_7.

Phonon-mediated superconductivity. Resistivity measurements are conducted in the vicinity of T_C with the application of magnetic fields perpendicular to the electric current, which provides additional evidence for the superconductivity in pressurized Re_3Ge_7. Figure 4(a) displays the temperature-dependent resistivity from 0–1.7 T at 17 GPa. With the increase of magnetic field, T_C monotonously shifts to lower temperature, which is typical for a bulk superconducting order. The superconducting phase is fully suppressed to below 1.8 K with a magnetic field of approximately 1.7 T. The

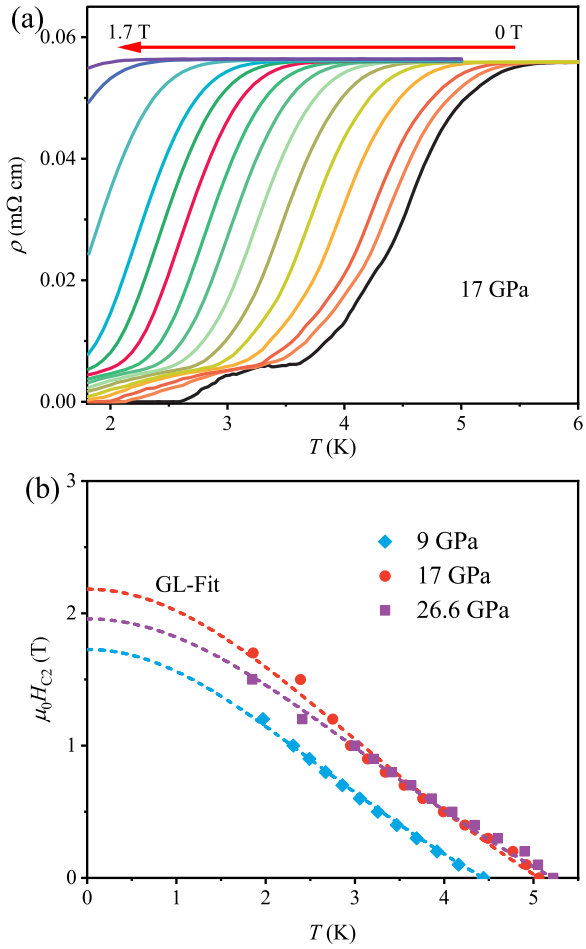

FIG. 4. The upper critical field determination of pressure-induced superconductivity in Re_3Ge_7. (a) Electrical resistivity as a function of temperature at 17 GPa under various magnetic fields from 0–1.7 T. (b) Temperature dependence of the upper critical field $\mu_0 H_{C2}$ for Re_3Ge_7 at 9 GPa, 17 GPa, and 26.6 GPa. The dashed curves represent the fitting results from Ginzburg-Landau equation.

upper critical fields $\mu_0 H_{C2}$ as a function of critical temperature at selected 9 GPa, 17 GPa, and 26.6 GPa are presented in Fig. 4(b). The experimental data can be well fitted via the Ginzburg-Landau equation [42]:

$$\mu_0 H_{C2}(T) = \mu_0 H_{C2}(0)\frac{1-(T/T_c)^2}{1+(T/T_c)^2} \tag{3}$$

The fitting results, shown as dashed curves in Fig. 4(b), yield zero-temperature $\mu_0 H_{C2}(0)$ of 1.73 T, 2.18 T, and 1.96 T at 9 GPa, 17 GPa, and 26.6 GPa, respectively. It is apparent that $\mu_0 H_{C2}(0)$ essentially follows similar trend to that of T_C varying with pressure. Furthermore, the coherence length $\xi(0)$ can be derived from the equation as follows:

$$\xi(0)^2 = \frac{\Phi_0}{2\pi\mu_0 H_{C2}(0)} \tag{4}$$

where $\Phi_0 = h/2e$ represents the magnetic flux quantum. As the pressure rises, the calculated $\xi(0)$ are 137.9, 122.9, and 129.6 Å for the pressures of 9, 17, and 26.6 GPa, respectively. The $\mu_0 H_{C2}(0)$ values are clearly lower than the Pauli-paramagnetic limit of $\mu_0 H_P = 1.84 \times T_C = 8 \sim 9$ T,

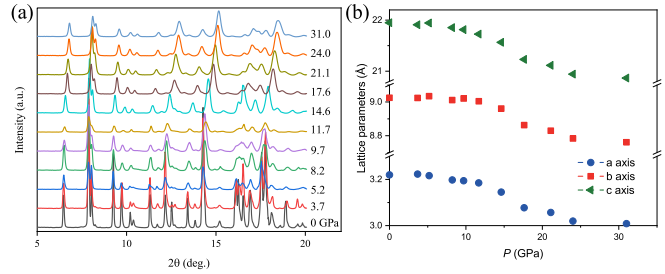

FIG. 5. High-pressure synchrotron XRD analysis of Re_3Ge_7. (a) XRD patterns of Re_3Ge_7 from ambient pressure up to 31 GPa. (b) Pressure dependence of lattice constants.

which describes the Zeeman effect destroying the Cooper pair in a weak-coupling Bardeen-Cooper-Schrieffer superconductor [43,44]. The quasilinear feature of temperature-dependent $\mu_0 H_{C2}$ highlights the substantial spin-orbital coupling participation to the superconductivity state, which might boost the Pauli-paramagnetic pair-breaking process [45]. In addition, the effectiveness of the Pauli-paramagneitc pair-breaking effect confirms phonon-mediated superconductivity Cooper-pair formation.

Pressure-temperature phase diagram. The typical synchrotron angle-dispersive XRD patterns of Re_3Ge_7 at different pressures are shown in Fig. 5(a). All diffraction peaks can be well indexed with the orthorhombic structure. With increased pressure, the peaks gradually shift to higher angles, implying lattice contraction under compression. The broadening of diffraction peaks due to the pressure gradient lead to some overlapping at high pressures, however, no new peaks appear up to 31 GPa. The orthorhombic structure is evidently well preserved within the pressure range, indicating outstanding structural stability. Figure 5(b) depicts the extracted lattice constants. A noticeable characteristics is the sharp decline of a, b, and c between 10 GPa and 20 GPa, which may indicate a rapid collapse of the lattice in this pressure range.

The competition between charge-ordered phase and superconductivity is demonstrated as a pressure-temperature (P-T) phase diagram in Fig. 6, which is summarized according to the aforementioned findings in two runs of high-pressure transport experiments. Orthorhombic Re_3Ge_7 does not undergo structure transitions under high pressure according to the synchrotron XRD patterns. The critical temperature of the charge-ordered state steadily falls as pressure increases. A relatively low pressure of 0.2 GPa allows for the emergence of bulk superconductivity, coexist with charge order up to around 5 GPa. The superconductivity exists in an unusual platform-shaped range up to experimentally achieved 38 GPa with no sign of abating, while the charge-ordered state collapses rapidly below ∼5 GPa. In general, the pressure typically triggers the phonon stiffening. Therefore in the scenario of phonon-mediated superconductivity, the unusual pressure-independent value of T_C would inevitably necessitate a delicate balance of parameters and unconventional electronic participation.

There is a connection between the charge-ordered state and superconductivity in the P-T phase diagram. This relationship is similar to the competitive relationship between the CDW/spin density wave (SDW) or antiferromagnetism

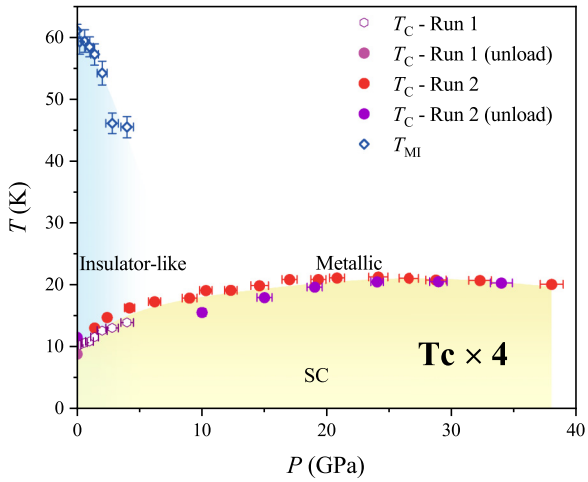

FIG. 6. Pressure-temperature electronic phase diagram of Re_3Ge_7. The dashed azure curve guides the boundary between the charge-ordered state and metallic state. The solid circle symbols represent the superconducting T_C in two runs. Note that the T_C data are multiplied by a factor of 4 for clarity.

(AFM) and superconductivity in high-temperature superconductors [1–3,9]. Potential origins of such low-temperature insulating state include the structure transition, CDW, Kondo effect, etc. [46–48]. The structure transition and Kondo effect are ruled out because the metal-insulator-like transition is second order and Re_3Ge_7 exhibits diamagnetism in the absence of magnetic impurities. In addition, the CDW signal was not detected in the low-temperature XRD patterns [49]. We also note that the previously speculated existence of the phonon-drag effect should not be the origin of the charge order, since the phonon-drag effect tends to reduce the electrical resistivity [29,50]. Verchenko *et al.* calculated the electronic structure of Re_3Ge_7 by density functional theory (DFT) [29], and stated that the transition to the semiconducting/metal state is accompanied by the opening of a band gap at the Fermi level right above the narrow pocket of hybridized states. However, in our ARPES measurement, the opening of a band gap at the Fermi level proposed in the calculation was not observed. Finally, after eliminating other possible origins, we note that all the experimental evidence points to an unconventional charge-driven state, possibly related to the electron correlation behavior. However, we note that some unconventional CDW orders in correlated materials cannot be directly probed by XRD or ARPES [51–53], whether the possible charge-driven state in Re_3Ge_7 belongs to such a category remains to be explored.

III. CONCLUSIONS

In summary, we present an ARPES and high-pressure transport investigation on Re_3Ge_7 single crystals with an unapprehended correlated charge-ordered ground state. The band structure of Re_3Ge_7 shows no obvious change after the metal-insulator-like transition. The high-pressure electrical resistivity measurement unveils that a robust superconducting state survives up to 38 GPa, with no apparent decrease in T_C. More importantly, the charge-ordered state is rapidly suppressed with increasing pressure, whereas the superconducting T_C is slightly enhanced simultaneously. Our work reveals the competing relationship between newly discovered unconventional charge order and superconductivity in Re_3Ge_7, with potential reference significance for understanding the electronic driven state and superconductivity in representative unconventional superconductors, which is certainly worthy of subsequent theoretical and experimental explorations.

IV. MATERIALS AND METHODS

Polycrystalline Re_3Ge_7 samples used for high-pressure synchrotron XRD experiments were prepared by the solid-state reaction method. High-purity Re (99.99%) and Ge (99.99%) powders were sealed in evacuated silica tubes and heated at 1123 K for 48 h. Single crystals of Re_3Ge_7 were grown via a Ge-rich self-flux method. Re and Ge were weighed in a molar ratio of 3:97 with a total mass of 2 g, placed in an alumina crucible and sealed in an evacuated quartz tube. The mixture was heated in a furnace to 1498 K and held at this temperature for 10 h. Finally, the furnace was cooled to 1173 K at a rate of 2.5 K/h. The crystals were separated from the flux by centrifuging. The structure of the crystals was determined by single-crystal x-ray diffraction with Mo Kα ($\lambda = 0.71073$ Å) radiation at room temperature using a Rigaku AtlasS2 diffractometer. The crystal was kept at 293(2) K during data collection. Using Olex2 [54], the structure was solved with the SHELXS structure solution program [55] using direct methods and refined with the SHELXL refinement package [56] using least-squares minimization.

The high-pressure electrical transport properties were measured by packing the sample in a screw-pressure-type made of nonmagnetic Be-Cu alloy. Pressure was calibrated by using the ruby fluorescence shift at room temperature. Platinum foils with a thickness of 10 μm were used for the standard five-probe method electrodes. High-pressure synchrotron XRD measurements were performed at beam line 15U1 ($\lambda = 0.6199$ Å) of the Shanghai Synchrotron Radiation Facility (SSRF, Shanghai).

Angle-resolved photoemission spectroscopy measurements were carried out on a laboratory system equipped with a Scienta R8000 analyzer. We use a helium discharge energy lamp as the light source that can provide photon of $h\nu = 21.218$ eV (He I). The Fermi level is referenced by measuring on a clean polycrystalline gold that is electrically connected to the sample. The crystals were cleaved *in situ* at 70 K with a base pressure of better than 8×10^{-11} Torr.

The data that support the findings of this study are available from the corresponding author upon reasonable request.

ACKNOWLEDGMENTS

This work was financially supported by the National Natural Science Foundation of China (Grants No. 12074360 and No. 12250410238) and the Frontier Scientific Research Program of Deep Space Exploration Laboratory under grant (No. 2022-QYKYJH-HXYF-019). The ARPES measurement was supported by the Fundamental Research Funds for the Central Universities (Grants No. WK3510000015

and No. WK3510000012), international partnership program of the Chinese Academy of Sciences (Grant No. 123GJHZ2022035MI), and the Innovation Program for Quantum Science and Technology (Grant No. 2021ZD0302802). High-pressure synchrotron XRD measurements were performed at beam line B15U1 ($\lambda = 0.6199$ Å) of Shanghai Synchrotron Radiation Facility (SSRF, Shanghai).

The authors declare no conflict of interest.

[1] N. P. Armitage, P. Fournier, and R. L. Greene, Progress and perspectives on electron-doped cuprates, Rev. Mod. Phys. **82**, 2421 (2010).

[2] E. Fradkin, S. A. Kivelson, and J. M. Tranquada, Colloquium: Theory of intertwined orders in high temperature superconductors, Rev. Mod. Phys. **87**, 457 (2015).

[3] P. C. Dai, Antiferromagnetic order and spin dynamics in iron-based superconductors, Rev. Mod. Phys. **87**, 855 (2015).

[4] E. Dagotto, Rev. Colloquium: The unexpected properties of alkali metal iron selenide superconductors, Rev. Mod. Phys. **85**, 849 (2013).

[5] P. F. S. Rosa, J. Kang, Y. Luo, N. Wakeham, E. D. Bauer, F. Ronning, Z. Fisk, R. M. Fernandes, and J. D. Thompson, Competing magnetic orders in the superconducting state of heavy-fermion $CeRhIn_5$, Proc. Natl. Acad. Sci. USA **114**, 5384 (2017).

[6] P. A. Lee, N. Nagaosa, and X.-G. Wen, Doping a Mott insulator: Physics of high-temperature superconductivity, Rev. Mod. Phys. **78**, 17 (2006).

[7] G. R. Stewart, Heavy-fermion systems, Rev. Mod. Phys. **56**, 755 (1984).

[8] H. Sun, M. Huo, H. Xunwu, J. Li, Z. Liu, Y. Han, L. Tang, Z. Mao, P. Yang, B. Wang, J. Cheng, D. Yao, G. Zhang, and M. Wang, Signatures of superconductivity near 80 K in a nickelate under high pressure, Nature (London) **621**, 493 (2023).

[9] E. E. M. Chia, J.-X. Zhu, D. Talbayev, R. D. Averitt, A. J. Taylor, K.-H. Oh, I.-S. Jo, and S.-I. Lee, Observation of competing order in a high-T_c superconductor using femtosecond optical pulses, Phys. Rev. Lett. **99**, 147008 (2007).

[10] N. D. Mathur, F. M. Grosche, S. R. Julian, I. R. Walker, D. M. Freye, R. K. W. Haselwimmer, and G. G. Lonzarich, Magnetically mediated superconductivity in heavy fermion compounds, Nature (London) **394**, 39 (1998).

[11] S. Uji, H. Shinagawa, T. Terashima, T. Yakabe, Y. Terai, M. Tokumoto, A. Kobayashi, H. Tanaka, and H. Kobayashi, Magnetic-field-induced superconductivity in a two-dimensional organic conductor, Nature (London) **410**, 908 (2001).

[12] E. Morosan, H. W. Zandbergen, B. S. Dennis, J. W. G. Bos, Y. Onose, T. Klimczuk, A. P. Ramirez, N. P. Ong, and R. J. Cava, Superconductivity in Cu_xTiSe_2, Nature Phys. **2**, 544 (2006).

[13] B. Sipos, A. F. Kusmartseva, A. Akrap, H. Berger, L. Forroó, and E. Tutiš, From Mott state to superconductivity in 1T-TaS_2, Nature Mater. **7**, 960 (2008).

[14] A. F. Kusmartseva, B. Sipos, H. Berger, L. Forró, and E. Tutiš, Pressure induced superconductivity in pristine 1T-TaS_2, Phys. Rev. Lett. **103**, 236401 (2009).

[15] J. P. Sun, K. Matsuura, G. Z. Ye, Y. Mizukami, M. Shimozawa, K. Matsubayashi, M. Yamashita, T. Watashige, S. Kasahara, Y. Matsuda, J.-Q. Yan, B. C. Sales, Y. Uwatoko, J.-G. Cheng, and T. Shibauchi, Dome-shaped magnetic order competing with high-temperature superconductivity at high pressures in FeSe, Nature Commun. **7**, 12146 (2016).

[16] H.-H. Kim, S. M. Souliou, M. E. Barber, E. Lefrancois, M. Minola, M. Tortora, R. Heid, N. Nandi, R. A. Borzi, G. Garbarino, A. Bosak, J. Porras, T. Loew, M. König, P. J. W. Moll, A. P. Mackenzie, B. Keimer, C. W. Hicks, and M. Le Tacon, Uniaxial pressure control of competing orders in ahigh-temperature superconductor, Science **362**, 1040 (2018).

[17] K. Y. Chen, N. N. Wang, Q. W. Yin, Y. H. Gu, K. Jiang, Z. J. Tu, C. S. Gong, Y. Uwatoko, J. P. Sun, H. C. Lei, J. P. Hu, and J.-G. Cheng, Double superconducting dome and triple enhancement of T_c in the Kagome superconductor CsV_3Sb_5 under high pressure, Phys. Rev. Lett. **126**, 247001 (2021).

[18] L. P. Gor'kov and V. Z. Kresin, Colloquium: High pressure and road to room temperature superconductivity, Rev. Mod. Phys. **90**, 011001 (2018).

[19] Z. Chi, X. Chen, F. Yen, F. Peng, Y. Zhou, J. Zhu, Y. Zhang, X. Liu, C. Lin, S. Chu, Y. Li, J. Zhao, T. Kagayama, Y. Ma, and Z. Yang, Superconductivity in pristine $2H_a$-MoS_2 at ultrahigh pressure, Phys. Rev. Lett. **120**, 037002 (2018).

[20] Z. Y. Liu, Q. X. Dong, P. T. Yang, P. F. Shan, B. S. Wang, J. P. Sun, Z. L. Dun, Y. Uwatoko, G. F. Chen, X. L. Dong, Z. X. Zhao, and J.-G. Cheng, Pressure-induced superconductivity up to 9 K in the quasi-one-dimensional KMn_6Bi_5, Phys. Rev. Lett. **128**, 187001 (2022).

[21] Q. Dong, J. Pan, S. Li, Y. Fang, T. Lin, S. Liu, B. Liu, Q. Li, F. Huang, and B. Liu, Record-high superconductivity in transition metal dichalcogenides emerged in compressed 2H-TaS_2, Adv. Mater. **34**, 2103168 (2022).

[22] L. Zheng, Z. Wu, Y. Yang, L. Nie, M. Shan, K. Sun, D. Song, F. Yu, J. Li, D. Zhao, S. Li, B. Kang, Y. Zhou, K. Liu, Z. Xiang, J. Ying, Z. Wang, T. Wu, and X. Chen, Emergent charge order in pressurized kagome superconductor CsV_3Sb_5, Nature (London) **611**, 682 (2022).

[23] P. Reiss, D. Graf, A. A. Haghighirad, W. Knafo, L. Drigo, M. Bristow, A. J. Schofield, and A. I. Coldea, Quenched nematic criticality and two superconducting domes in an iron-based superconductor, Nature Phys. **16**, 89 (2020).

[24] J. J. Hamlin, D. A. Zocco, T. A. Sayles, M. B. Maple, J. H. Chu, and I. R. Fisher, Pressure-induced superconducting phase in the charge-density-wave compound terbium tritelluride, Phys. Rev. Lett. **102**, 177002 (2009).

[25] T. Yamauchi, Y. Ueda, and J. Yamaura, Pressure-induced superconductivity in β-$Na_{0.33}V_2O_5$ beyond charge ordering, Phys. Rev. Lett. **89**, 057002 (2002).

[26] T. Siegrist, F. Hulliger, and W. Petter, The crystal structure of Re_3Ge_7, J. Less-Common Met. **90**, 143 (1983).

[27] A. Rabus and E. Mun, Anomalous transport properties of Re_3Ge_7, Phys. Rev. Mater. **3**, 013404 (2019).

[28] Y. Cui, S. Wu, Q. Zhu, G. Xiao, B. Liu, J. Wu, G. Cao, and Z. Ren, Metal-insulator-like transition, superconducting dome and topological electronic structure in Ga-doped Re_3Ge_7, npj Quantum Mater. **6**, 74 (2021).

[29] V. Yu. Verchenko, M. S. Likhanov, A. V. Mironov, and A. V. Shevelkov. Electronic phase transition in the Re_3Ge_7 endohedral cluster compound, Phys. Rev. B **106**, 195203 (2022).

[30] T. Zhang, Y. Jiang, Z. Song, H. Huang, Y. He, Z. Fang, H. Weng, and C. Fang, Catalogue of topological electronic materials, Nature (London) **566**, 475 (2019).

[31] See Supplemental Material at http://link.aps.org/supplemental/10.1103/PhysRevB.108.224504 for further details on the ARPES experimental results.

[32] Y. Zhang, C. Wang, L. Yu *et al.* Electronic evidence of temperature-induced Lifshitz transition and topological nature in $ZrTe_5$, Nature Commun. **8**, 15512 (2017).

[33] H. Chi, C. Zhang, G. Gu, D. E. Kharzeev, X. Dai, Q. Li, Lifshitz transition mediated electronic transport anomaly in bulk $ZrTe_5$, New J. Phys. **19**, 015005 (2017).

[34] S. L. Bud'ko, P. C. Canfield, C. H. Mielke, and A. H. Lacerda, Anisotropic magnetic properties of light rare-earth diantimonides, Phys. Rev. B **57**, 13624 (1998).

[35] P. M. Chaikin, Magnetic-field-induced transition in quasi-two-dimensional systems, Phys. Rev. B **31**, 4770 (1985).

[36] I. Palacio, J. Obando-Guevara, L. Chen, M. N. Nair, M. A. González Barrio, E. Papalazarou, P. Le Fèvre, A. Taleb-Ibrahimi, E. G. Michel, A. Mascaraque, and A. Tejeda, Fermi surface of $LaSb_2$ and direct observation of a CDW transition, Appl. Surf. Sci. **610**, 155477 (2023).

[37] E. Mun, S. L. Bud'ko, and P. C. Canfield, Robust tunability of magnetoresistance in half-Heusler RPtBi (R = Gd, Dy, Tm, and Lu) compounds, Phys. Rev. B **93**, 115134 (2016).

[38] T. Suzuki, R. Chisnell, A. Devarakonda, Y.-T. Liu, W. Feng, D. Xiao, J. W. Lynn, and J. G. Checkelsky, Large anomalous Hall effect in a half-Heusler antiferromagnet, Nature Phys. **12**, 1119 (2016).

[39] M. Kang, S. Fang, J.-K. Kim, B. R. Ortiz, S. H. Ryu, J. Kim, J. Yoo, G. Sangiovanni, D. D. Sante, B.-G. Park, C. Jozwiak, A. Bostwick, E. Rotenberg, E. Kaxiras, S. D. Wilson, J.-H. Park, and R. Comin, Twofold van Hove singularity and origin of charge order in topological kagome superconductor CsV_3Sb_5, Nature Phys. **18**, 301 (2022).

[40] Y. A. Gerasimenko, P. Karpov, I. Vaskivskyi, S. Brazovskii, and D. Mihailovic, Intertwined chiral charge orders and topological stabilization of the light-induced state of a prototypical transition metal dichalcogenide, npj Quantum Mater. **4**, 32 (2019).

[41] M. Zhang, X. Wang, A. Rahman, R. Dai, Z. Wang, and Z. Zhang, Cascade of phase transitions and Dirac revivals in magic-angle graphene, Phys. Rev. B **101**, 064106 (2020).

[42] J. A. Woollam, R. B. Somoano, and P. O. Connor, Positive curvature of the H_{c2} -versus-T_c boundaries in layered superconductors, Phys. Rev. Lett. **32**, 712 (1974).

[43] A. M. Clogston, Upper limit for the critical field in hard superconductors, Phys. Rev. Lett. **9**, 266 (1962).

[44] B. S. Chandrasekhar, a note on the maximum critical field of high-field superconductors, Appl. Phys. Lett. **1**, 7 (1962).

[45] N. R. Werthamer, E. Helfand, and P. C. Hohenberg, Temperature and purity dependence of the superconducting critical field H_{c2}.III. electron spin and Spin-Orbit effects, Phys. Rev. **147**, 295 (1966).

[46] C. S. Alexander, G. Cao, V. Dobrosavljevic, S. McCall, J. E. Crow, E. Lochner, and R. P. Guertin, Destruction of the Mott insulating ground state of Ca_2RuO_4 by a structural transition, Phys. Rev. B **60**, R8422(R) (1999).

[47] X. Xu, A. F. Bangura, J. G. Analytis, J. D. Fletcher, M. M. J. French, N. Shannon, J. He, S. Zhang, D. Mandrus, R. Jin, and N. E. Hussey, Directional field-induced metallization of quasi-one-dimensional $Li_{0.9}Mo_6O_{17}$, Phys. Rev. Lett. **102**, 206602 (2009).

[48] Y. Matsushita, H. Bluhm, T. H. Geballe, and I. R. Fisher, Evidence for Charge Kondo effect in superconducting Tl-doped PbTe, Phys. Rev. Lett. **94**, 157002 (2005).

[49] F. B. Carneiro, L. S. I. Veiga, J. R. L. Mardegan, R. Khan, C. Macchiutti, A. López, and E. M. Bittar, Unveiling charge density wave quantum phase transitions by x-ray diffraction, Phys. Rev. B **101**, 195135 (2020).

[50] R. P. Huebener, Effect of phonon drag on the electrical resistivity of metals, Phys. Rev. **146**, 502 (1966).

[51] U. Chatterjee, M. Shi, A. Kaminski, A. Kanigel, H. M. Fretwell, K. Terashima, T. Takahashi, S. Rosenkranz, Z. Z. Li, H. Raffy, A. Santander-Syro, K. Kadowaki, M. R. Norman, M. Randeria, and J. C. Campuzano1, Nondispersive Fermi arcs and the absence of charge ordering in the pseudogap phase of $Bi_2Sr_2CaCu_2O_8$, Phys. Rev. Lett. **96**, 107006 (2006).

[52] E. H. da Silva Neto, P. Aynajian, A. Frano, R. Comin, E. Schierle, E. Weschke, A. Gyenis, J. Wen, J. Schneeloch, Z. Xu, S. Ono, G. Gu, M. L. Tacon, and A. Yazdani, Ubiquitous interplay between charge ordering and high-temperature superconductivity in Cuprates, Science **343**, 393 (2014).

[53] M. Hashimoto, G. Ghiringhelli, W.-S. Lee, G. Dellea, A. Amorese, C. Mazzoli, K. Kummer, N. B. Brookes, B. Moritz, Y. Yoshida, H. Eisaki, Z. Hussain, T. P. Devereaux, Z.-X. Shen, and L. Braicovich, Magnetic-field-induced transition in quasi-two-dimensional systems, Phys. Rev. B **89**, 220511(R) (2014).

[54] O. V. Dolomanov, L. J. Bourhis, R. J. Gildea, J. A. K. Howard, and H. Puschmann, OLEX2: A complete structure solution, refinement and analysis program, J. Appl. Cryst. **42**, 339 (2009).

[55] G. M. Sheldrick, SHELX-97-Programs for crystal structure determination (SHELXS) and refinement (SHELXL), Acta Cryst. A **64**, 112 (2008).

[56] G. M. Sheldrick, Crystal structure refinement with SHELXL, Acta Cryst. C **71**, 3 (2015).